JOURNAL OF PROPULSION AND POWER
Vol. 11, No. 3, May–June 1995

Analysis and Testing of Propellant Feed System Priming Process

T. Y. Lin*
McDonnell Douglas Aerospace, Huntington Beach, California 92647
and
D. Baker†
NASA Johnson Space Flight Center, Las Cruces, New Mexico 88004

This article presents analytical and experimental results on the priming of a propellant feed system with initial line pressures of 0 psia and greater. The analysis employs the method of characteristics to treat one-dimensional liquid transients in liquid-full segments, and the lumped-inertia technique to model the dynamics of partially filled (or two-phase) segments. Fluid compressibility and piping flexibility are accounted for, and the method of characteristics can undertake a complex system. The highly significant correlation obtained between predictions and test results verifies that the methods are suitable for analyzing a complicated network system.

Nomenclature

A = area of pipe
a = speed of pressure pulse
B = bulk modulus of elasticity of fluid
C_f = critical flow coefficient
C_v = flow coefficient for valves; flow rate is expressed in gal/min of 60°F water with a 1-psi pressure drop across the valve
c = dimensionless parameter that describes the effect of the pipe constraint condition on the wave speed
D = pipe diameter
E = modulus of elasticity
e = pipe wall thickness
F = pressure force
f = Darcy–Weisbach friction factor
g = gravitational acceleration
H = piezometric head
K = minor loss coefficient in the formula, $\Delta H = K(V^2/2g)$
k = specific heat ratio
n = polytropic exponent
P = pressure
Q = flow rate
t = time
V = velocity
$\forall$ = volume
X = length of the liquid column within a segment
x = distance along the pipe
z = elevation of the pipe above datum
α = pipe slope
Δ = difference between two points
ρ = density
τ = percent opening of a valve

Subscripts
B = barometric
C = point C in the xt plane of the characteristics grid
f = friction
i = segment number
P = point P in the xt plane of the characteristics grid
0 = previous time

Introduction

PRIMING a liquid-propellant feed system in orbit could create surge pressures that could result in an explosion or damage to the feed line.[1] There are two mechanisms that create hazards during the priming process. One is the rapid compression of inert gas or propellant vapor that generates heat and causes explosive decomposition of the propellant. The other is the water-hammer pressure generated when the liquid propellant impacts the closed thruster valve or other dead-ended valves and fittings.

To prevent these two potential hazards, the solution is to slow down the priming flow through the use of either a flow restriction device or the gas cushion effect as demonstrated in Refs. 2 and 3. However, the addition of flow restriction devices may significantly increase the system pressure loss, and also the compressed high-pressure gas, which eventually has to be vented out, and may damage the downstream components that were not originally designed to withstand a high pressure gas fow. Apparently there is a need for analyzing the priming flow phenomena and, thus, defining a method to reduce surge pressure without compromising the system performance requirements.

This article presents a comparison of theory with experimental data for basic feed line configurations such as straight lines, elbow, and tees; as well as for a network system. The agreement in comparison ensures that the math model presented here can be used to predict the system performance characteristics, to size a flow restriction device, and to produce a safe and reliable system. Note that this article did not consider any chemical reactions in the analysis because a reduction of water-hammer pressure will certainly eliminate the potential of explosion.

Analysis

Two approaches have been used to analyze the adiabatic compression associated with the priming process. One approach used the lumped-inertia technique that solves only the

Presented as Paper 92-3315 at the AIAA/SAE/ASME/ASEE 28th Joint Propulsion Conference and Exhibit, Nashville, TN, July 6–8, 1992; received July 27, 1992; revision received Jan. 4, 1994; accepted for publication April 7, 1994.

*Principal Engineer/Scientist, Space Station Division. Member AIAA.
†Laboratory Office, White Sands Test Facility. Member AIAA.

equation of motion.[4] This approach considers the inertial effect, but the elastic properties of the fluid and pipe wall are neglected. The other approach used the lumped-capacitance technique that solves only the continuity equation. The momentum equation is treated as a simple steady-state pressure-drop equation. This approach considers the elastic effects; however, the inertial effect is absent.

This article describes a new approach that encompasses a full treatment of the one-dimensional fluid transient equations, with the lumped-inertia treatment for two-phase segments. The solution method employs the method of characteristics that is suitable for solving a network system. In addition, the fluid choking effect and a nonlinear characteristics tee junction model are included. Previous papers[4,5] neglected the choking effect and concentrated on the friction factor for explaining the discrepancy between the measured and predicted fluid impact time. The tee junction model is essential for the network priming flow simulation and plays a vital part in directing the priming flow throughout the network. Prickett et al.[5] presented the network priming flow test; however, in their network flow analysis, only symmetric flow branching was discussed. The treatment of equal branch flow is inadequate for a network flow analysis because the tee orientation to flow direction, such as a branch-tee or run-tee, and flow resistance of the flow path dictate the branch flow rates.

Basic Equations for Liquid Transient Flow

The water-hammer phenomenon in pipes is commonly described by a one-dimensional model with the following equations[6]:

the equation of motion

$$g\frac{\partial H}{\partial x} + \frac{dV}{dt} + \frac{fV|V|}{2D} = 0 \tag{1}$$

and the continuity equation

$$\frac{a^2}{g}\frac{\partial V}{\partial x} + V\left(\frac{\partial H}{\partial x} + \sin\alpha\right) + \frac{\partial H}{\partial t} = 0 \tag{2}$$

where the total derivative following the motion of the fluid is given by

$$\frac{d}{dt} = V\frac{\partial}{\partial x} + \frac{\partial}{\partial t}$$

and a can be expressed for a circular pipe as

$$a = \sqrt{\frac{B/\rho}{1 + (B/E)(D/e)c}} \tag{3}$$

Equations (1) and (2) can be transformed into a pair of ordinary differential equations, through the method of characteristics, which are grouped and identified as C^+ and C^- equations

$$C^+: \begin{cases} \frac{g}{a}\frac{dH}{dt} + \frac{dV}{dt} + \frac{g}{a}V\sin\alpha + \frac{fV|V|}{2D} = 0 \\ \frac{dx}{dt} = V + a \end{cases} \tag{4}$$

$$C^-: \begin{cases} -\frac{g}{a}\frac{dH}{dt} + \frac{dV}{dt} - \frac{g}{a}V\sin\alpha + \frac{fV|V|}{2D} = 0 \\ \frac{dx}{dt} = V - a \end{cases} \tag{5}$$

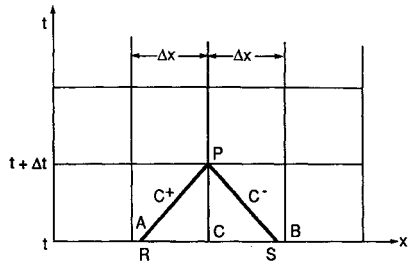

Fig. 1 Method of specified time intervals.

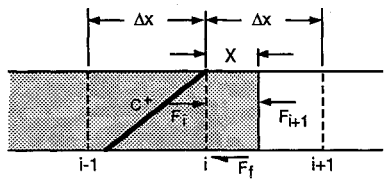

Fig. 2 Treatment of two-phase segment.

In finite difference form, the characteristic equations become

$$C^+: V_P = C_3 - C_2H_P \tag{6}$$

$$C^-: V_P = C_1 + C_2H_P \tag{7}$$

where

$$C_1 = V_S[1 + C_2\Delta t\sin\alpha - (f\Delta t/2D)|V_s|] - C_2H_s$$

$$C_2 = g/a$$

$$C_3 = V_R[1 - C_2\Delta t\sin\alpha - (f\Delta t/2D)|V_R|] + C_2H_R$$

By use of the specified-time-intervals method with conditions known at A, B, and C (Fig. 1), a linear interpolation can be used to find the conditions at points R and S. Then Eqs. (6) and (7) can be solved for the unknowns V_P and H_P at time $t + \Delta t$ from the known values at the points R and S at time t.

Two-Phase Segment

The equation of motion is used to describe the dynamics of a two-phase or partially liquid-filled segment. The equation is solved simultaneously with the C^+ characteristics equation for $V_{P,i}$ and $H_{P,i}$. The equations are

$$V_{P,i} = C_3 - C_2H_{P,i} \tag{6'}$$

$$F_i - F_{i+1} - F_f = (\rho A_i X)\frac{dV_i}{dt} \tag{8}$$

With a second-order approximation, the pressure force (shown in Fig. 2) equations become

$$F_i = \tfrac{1}{2}\rho g A_i(H_{P,i} + H_{C,i}) \tag{9}$$

$$F_{i+1} = \tfrac{1}{2}\rho g A_i(H_{P,i+1} + H_{C,i+1}) \tag{10}$$

$$F_f = (f\rho XV|V|A_i/2D) \tag{11}$$

$$X = \tfrac{1}{2}(X_{C,i} + X_{P,i}) \tag{12}$$

$$V = \tfrac{1}{2}(V_{C,i} + V_{P,i}) \tag{13}$$

$$\frac{dV_i}{dt} = \frac{(V_{P,i} - V_{C,i})}{\Delta t} \tag{14}$$

For the pressurized line, the gas is idealized to satisfy the reversible polytropic relation

$$(H_{P,i+1} - z + H_B)\forall^n = C \tag{15}$$

For a perfect gas, limiting values of n hold for an isothermal process $n = 1$, and an isentropic process $n = k$. The gas volume $\forall$ is determined by

$$\forall = \forall_0 - \tfrac{1}{2}\Delta t A_i(V_{C,i} + V_{P,i}) \tag{16}$$

Equations (6′) and (9–16) can be substituted into Eq. (8) to obtain a nonlinear equation in the variable $V_{P,j}$. This nonlinear equation is solved by Newton's method to obtain $V_{P,i}$. The value of $H_{P,i}$ is then calculated from Eq. (6′).

Boundary Conditions

Wylie and Streeter[6] describe the basic boundary conditions for tanks, pipe ends, valves, and junctions. The water-hammer pressure P_{wh}, when the liquid column is brought to a stop at a dead end is determined by

$$P_{wh} = (\rho a v/144g) \tag{17}$$

where v is the liquid velocity at the time of impact.

The following sections describe the valve boundary with and without cavitation flow and the tee junction boundary with flow-dependent branching losses.

Valve Equations

Equation (6), describing the flow characteristics upstream of the valve, and Eq. (7), describing the characteristics downstream of the valve, are solved simultaneously with the valve flow equation (Fig. 3). The three basic equations describing the boundary are

$$V_{P,i} = C_{3,i} - C_{2,i}H_{P,i} \tag{6″}$$

$$V_{P,i+1} = C_{1,i+1} + C_{2,i+1}H_{P,i+1} \tag{7′}$$

$$Q = \tau C_v\sqrt{(\Delta P 62.4/\rho g)} \tag{18}$$

Combining the above three equations results in a quadratic equation, which may be solved to yield Q. The upstream and downstream pressure heads at the valve are then obtained from Eqs. (6″) and (7′).

For the choked flow situation, in which the pressure difference across the valve is greater than the product of the square of the critical flow factor and the difference between upstream pressure and vapor pressure, the following equation is used in lieu of Eq. (18)

$$Q = \tau C_v C_f\sqrt{(\Delta P_v 62.4/\rho g)}$$

where ΔP_v is the pressure difference between the valve upstream pressure and the fluid vapor pressure.

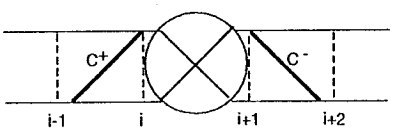

Fig. 3 Valve in line.

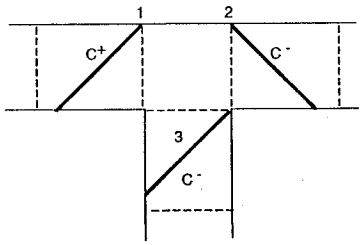

Fig. 4 Tee junction.

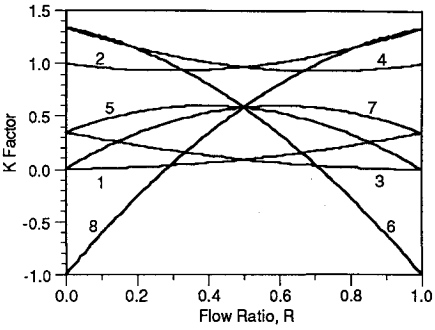

	Flow Ratio, R	K Factor Curve Number	
1 → 2, ↓3	Q3/Q1	K12	K13
		1	2
← , ↓	Q1/Q2	K21	K23
		3	4
← , ↑	Q1/Q3	K31	K32
		2	4
→ , ↑	Q1/Q2	K12	K32
		5	6
← , ↑	Q3/Q1	K21	K31
		7	8
→ , ↓	Q1/Q3	K13	K23
		2	4

Fig. 5 Pressure loss K-factor for tee junction.

Tee Junction Pressure Loss

The tee junction can be treated as a zero-pressure-loss junction or a junction with pressure loss generated from mixing or separation of flow. With no pressure loss, three characteristic equations are sufficient to describe the boundary

$$V_{P,1} = C_{3,1} - C_{2,1}H_{P,1} \tag{19}$$

$$V_{P,2} = C_{1,2} + C_{2,2}H_{P,2} \tag{20}$$

$$V_{P,3} = C_{1,3} + C_{2,3}H_{P,3} \tag{21}$$

where subscript 1 indicates the tee inlet conditions; subscript 2, the conditions at the downstream branch; and subscript 3, the conditions at the lateral branch (Fig. 4). With the consideration of mass balance at the junction, the above three equations can be solved for the pressure head at the junction

$$H_{P,1} = H_{P,2} = H_{P,3} = \frac{(A_1C_{3,1} + A_2C_{1,2} + A_3C_{1,3})}{(A_1C_{2,1} - A_2C_{2,2} - A_3C_{2,3})} \tag{22}$$

The velocities $V_{P,1}$, $V_{P,2}$, and $V_{P,3}$ are then determined from Eqs. (19–21).

With flow-dependent branching losses, two equations are needed to describe the relationships among $H_{P,1}$, $H_{P,2}$, and $H_{P,3}$. Vazsonyi[7] presented the pressure-loss equations for separating and uniting flows at the tee junction. These equations were derived on a theoretical and experimental basis. Figure 5 presents K-factor vs flow ratio for the six possible flows at the tee junction. These are the result of modifications to the Vazsonyi equations in order to have agreements in the K-factors when the flow ratio is approaching zero or unity.

The formulas used to generate Fig. 5 are as follows:

for separating flow from the tee

$$\Delta H_{12} = (c_1V_{P,1}^2 + c_1V_{P,2}^2 - c_2V_{P,1}V_{P,2})/g \tag{23}$$

$$\Delta H_{13} = (c_3V_{P,1}^2 + c_4V_{P,3}^2 - c_5V_{P,1}V_{P,3})/g \tag{24}$$

and for uniting flow into the tee

$$\Delta H_{12} = (c_3V_{P,2}^2 + (c_3 - A_{12})V_{P,1}^2 - c_6A_{32}V_{P,3}^2)/g \tag{25}$$

$$\Delta H_{32} = (c_3V_{P,2}^2 + (c_3 - c_6A_{32})V_{P,3}^2 - A_{12}V_{P,1}^2)/g \tag{26}$$

Table 1 Summary of analysis

Test section	Test no.	Tank pressure, psia	Line pressure, psia	Valve opening time, ms	Peak surge time		Peak pressure		
					Test, ms	Predicted, ms	Test, psia	Predicted, psia	Percent difference
Vacuum cases									
10-in. line	21	435	0.0024	145.0	128.5	127.4	3965	4725	19
20-in. line	24	413	0.0019	146.7	140.7	138.8	5467	5870	7
30-in. line	26	407	0.0019	144.0	147.0	147.0	6450	6400	−1
10- × 10-in. elbow	65	416	0.0019	143.8	138.7	140.6	5096	5770	13
10- × 10- × 10-in. tee (right/left)	36	415	0.0019	144.2	148.2, left	149.0	6090	6190	2
					149.2, right	149.0	6980	6190	−11
10- × 10- × 10-in. tee (bottom/side)	47	411	0.0019	142.8	147.6, bottom	146.0	5120	6900	35
					146.0, side	146.0	6990	7030	1
10- × 20- × 20-in. tee (bottom/side)	51	412	0.0019	142.7	165.3, bottom	162.2	5600	6860	23
					157.5, side	162.0	6470	6600	2
Ambient cases									
10-in. line	18	405	12.7	145.3	129.4	128.2	2241	1670, adiabatic	−26
						128.4		3170, isothermal	42
20-in. line	16	410	12.7	144.6	139.0	139.0	3458	2467, adiabatic	−29
						139.5		4320, isothermal	25
30-in. line	29	412	12.7	142.8	146.7	146.2	4016	2922, adiabatic	−27
						147.2		4872, isothermal	21
10- × 10-in. elbow	61	410	12.7	145.7	141.8	142.0	2600	2150, adiabatic	−17
						142.6		4043, isothermal	56
10- × 10- × 10-in. tee (right/left)	34	410	12.7	144.0	149.7, left	149.7	2750	2000, adiabatic	−27
						150.0		3823, isothermal	39
					149.8, right	149.7	2840	2000, adiabatic	−30
						150.0		3823, isothermal	39
10- × 10- × 10-in. tee (bottom/side)	40	409	12.7	141.8	148.0, bottom	149.0	4180	4000, adiabatic	−4
					148.8, side	151.4	5100	2700, adiabatic	−47
10- × 20- × 20-in. tee (bottom/side)	55	412	12.7	139.7	162.5, bottom	167.0	3000	3370, adiabatic	12
					164.5, side	162.0	2100	2340, adiabatic	11

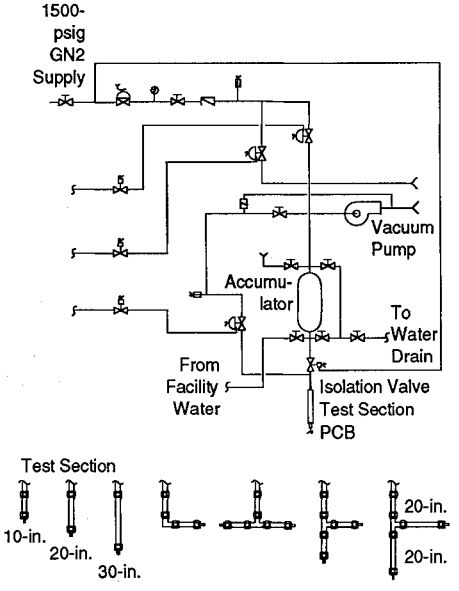

Fig. 6 Test setup and test sections.

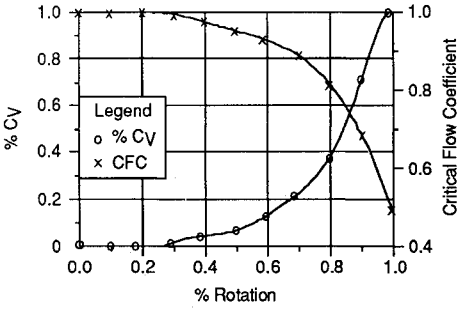

Fig. 7 Valve characteristics of Jamesbury ball valve.

where $c_1 = 0.1714$, $c_2 = 0.3428$, $c_3 = 0.5$, $c_4 = 0.4$, $c_5 = 0.2285$, $c_6 = 0.3285$, A_{12} is the area ratio of A_1 to A_2, and A_{32} is the area ratio of A_3 to A_2.

The two pressure-loss equations, either from separating flow or uniting flow, and the three characteristic equations [Eqs. (19–21)] can be reduced to two nonlinear equations containing only the variables of downstream and lateral flow velocities. These two nonlinear equations are then solved for the two velocities. The main flow rate is then determined, and the three junction pressure heads are calculated from Eqs. (19–21).

Testing

Basic feed line configurations such as straight line, elbow, and tee were tested in order to provide experimental data for a math model verification. Figure 6 shows the schematics of the test setup and seven test sections (consisting of $\frac{1}{2}$-in. stainless steel tubing), which include 10-, 20-, and 30-in. straight lines; a 10- by 10-in. 90-deg elbow; a right/left arranged 10- by 10- by 10-in. tee; and two bottom/side arranged tees: one with a dimension of 10- by 10- by 10-in., and the other with 10- by 20- by 20-in. The test setup consisted of an accumulator with a capacity of 4 gal, an isolation valve, and a test section with pressure transducer(s) located at its dead end(s). The isolation valve was a $\frac{1}{2}$-in. pneumatically activated Jamesbury ball valve. Figure 7 presents the valve characteristics of the flow coefficient ($\%C_v$) and critical flow coefficient.[8] The flow coefficient is 8.3 at the valve's full open position.

Prior to the test, the system was filled with water from the upstream side of the isolation valve to the halfway point of the accumulator. The accumulator pressure was established at approximately 400 psia, and the test section was then either evacuated to a pressure as low as 0.1 torr or pressurized at

ambient pressure (12.7 psia at test site) with nitrogen gas. By opening the isolation valve, the high-pressure water will either impact the dead end(s) of the test section (for the initial vacuum case) or compress the inert gas inside the test section (for the initial ambient case). The pressure profile(s) at the dead end(s) and the valve opening time were recorded during the tests. The surge pressures were measured by the high-response piezoelectric dynamic pressure transducers (PCB). The recorded valve opening time varied around 144 ms, which covers the period between the instant when the valve opening signal was sent and the instant when the valve position indicator switch was activated.

Analysis and Test Results

A highly significant correlation between predictions and test results was obtained as shown in Table 1 that summarizes the analysis and test results for the initial vacuum and ambient cases. The predicted peak surge occurrence times agree very well with test results; most of the differences are less than 2 ms. The percentage difference between predicted and measured peak pressure ranges from -11 to 19% for the straight line, elbow, and right/left arranged tee cases with initial vacuum. For the initial ambient cases, the peak surge pressure measurements fell between the adiabatic and isothermal predictions. The adiabatic predictions were generally 20–30% below the test results.

For the bottom/side arranged tee with initial vacuum, there are good agreements (1–2% difference) in peak surge pressure for side branch, however, for the bottom branch, the predictions are 23–35% higher than the test results. By examining the test data, one may conclude that this is due to the released gas bubbles during fill-up of the bottom branch, that increase the fluid compressibility. For the initial ambient case, the predictions deviated somewhat from test results by the rapid flow oscillation between branches and by the fact that the short branch gas volumes may not stay in places during surge cycles as one may expect.

The following sections compare pressure histories for straight line (30-in.), right/left arranged tee, and bottom/side arranged tee (10- by 20- by 20-in.) cases. The 10- by 10-in. 90-deg elbow case did show similar pressure surge effects, as compared with the 20-in. straight line case, but only with diminished surge pressures due to energy dissipation at the elbow, therefore, a detailed comparison was not presented. Finally, test repeatability will be discussed along with the predictions of the network experiment conducted by Prickett et al.[5]

Straight Line

Test results show a progressive increase in surge pressures for the 10-, 20-, and 30-in. line test sections both for the initial vacuum and ambient cases. This is due to the relatively slow opening of the valve; only in the 30-in. line test case was the ball valve fully opened before the peak surge occurred. An excellent correlation between the measured and predicted peak surge occurrence times for all three cases leads to the conclusions that the ball-valve model was accurate in predicting flow rate, and the valve flow coefficient became the dominant factor on peak surge pressure. Note the valve opening time should not affect the surge pressure further when the manifold fill time is greater than the valve opening time.

Figure 8 compares the pressure histories for the 30-in. line with an initial vacuum. The figure shows that the predicted and measured peak surge pressures and occurrence times were almost identical.

Analytically, when the one-dimensional water flow impacts the dead end, an initial surge is generated instantaneously according to Eq. (17). This surge pressure wave then propagates upstream to stop the water flow at a speed depending on the fluid's compressibility and the elasticity of the tube's material as shown in Eq. (3). Since upstream pressure is always greater than downstream pressure before the impact, the surge pressure will continuously increase in order to bring the fluid flow to rest. This creates other surges on top of the initial one when the wave passes through restrictions such as valves. The duration of the peak surge measured at the pipe end is twice the time required for the wave to travel from the pipe end to the tank.

The test data shows there were small surges before the peak surge, and the peak surge's duration was less than expected. This is an indication that water flow did not develop fully (as a one-dimensional flow) due to a short line length, the opening of the valve, and a choked flow situation within the valve. The vertical orientation of the test setup did not help either, because gravity enhanced the separation of water flow. Thus, the final water flow impacted the water already accumulated at the pipe end, contributing to the shape and duration of the peak surge pressure. As the water column bounced back after the first peak surge and hit the pipe end for the second time, the surge pressure shape and duration resembled the analytical predictions of the first surge.

For the initial ambient pressure case, Fig. 9 compares the test and the analytical results for the 30-in. line test section, which include the adiabatic and isothermal predictions. The measured peak surge pressure fell between the adiabatic and isothermal predictions. With ambient pressure gas in the test

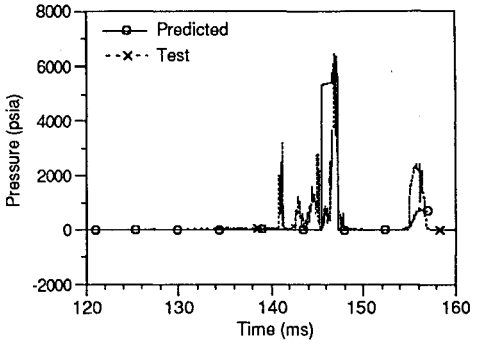

Fig. 8 30-in. line comparison (initially at vacuum pressure).

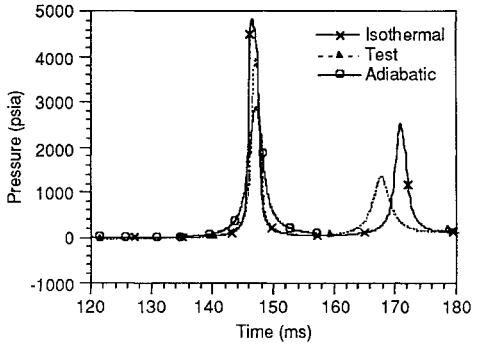

Fig. 9 30-in. line comparison (initially at ambient pressure).

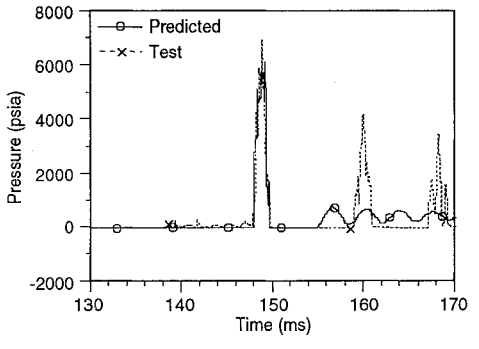

Fig. 10 Right-branch comparison (10- × 10- × 10-in. tee initially at vacuum pressure).

section, the surge pressure is expected to be less because the inert gas provides a cushion for the accelerating water column. One should expect the gas compression process to be close to the adiabatic process in light of the ms time scale, however, the mixing of water with gas (caused by a not fully developed flow) and the possible loss of gas back to the accumulator during the surge cycle will certainly contribute to the deviation from the adiabatic process.

Right/Left Arranged Tee

For the right/left arranged tee, the water flow splits evenly into each branch and impacts the dead ends at the same time. This produces identical initial surge pressures (approximately 3000 psia in the solid lines shown in Figs. 10 and 11), which are then amplified by wave propagations and interactions between branches, and lead to higher final peak surge pressures for both branches (approximately 6200 psia). Figures 10 and 11 show that the predicted pressure profiles are close to the test results for both branches. The predicted peak pressure is 11% lower than the right-branch test result, and is 2% higher than the left-branch test result. Note that the average peak

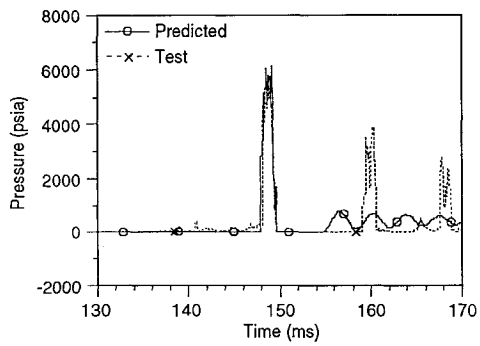

Fig. 11 Left-branch comparison (10- × 10- × 10-in. tee initially at vacuum pressure).

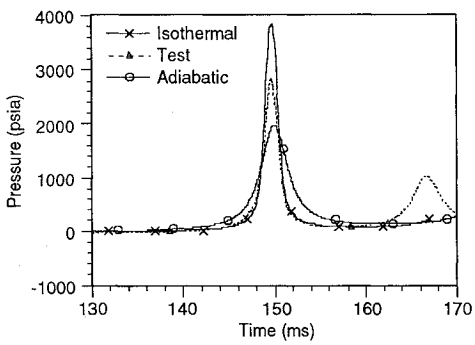

Fig. 12 Right-branch comparison (10- × 10- × 10-in. tee initially at ambient pressure).

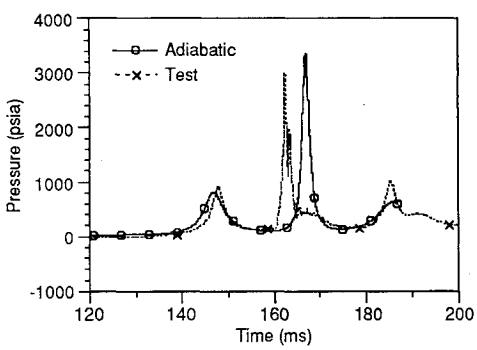

Fig. 13 Bottom-branch comparison (10- × 20- × 20-in. tee initially at ambient pressure).

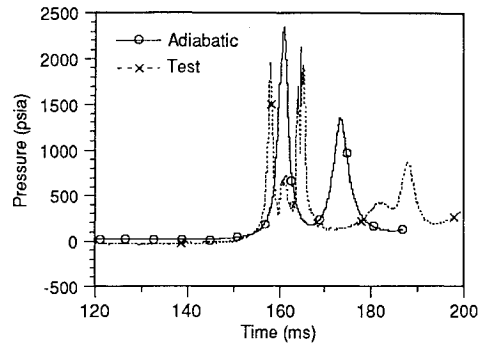

Fig. 14 Side-branch comparison (10- × 20- × 20-in. tee initially at ambient pressure).

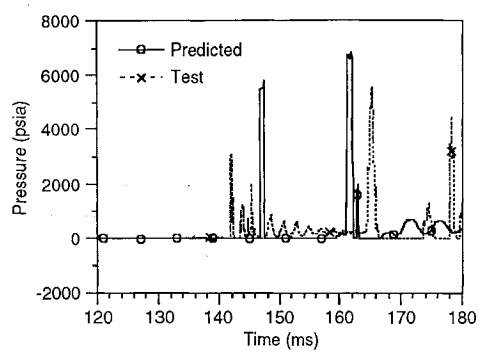

Fig. 15 Bottom-branch comparison (10- × 20- × 20-in. tee initially at vacuum pressure).

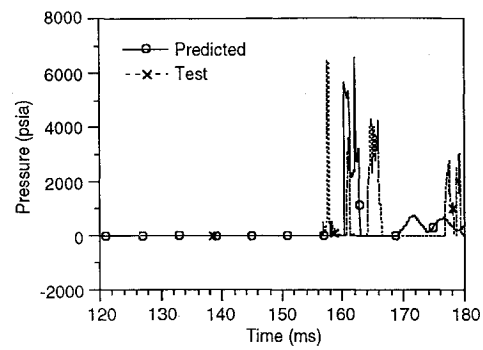

Fig. 16 Side-branch comparison (10- × 20- × 20-in. tee initially at vacuum pressure).

branch pressure of this tee configuration is close to that of the 30-in. line case, despite the fact that the branch flow was half of the main flow.

For the initial ambient case, the inert gas in the branches provides two equal cushions for the water flow in the branches. Figure 12 compares pressure histories for the right branch (the left branches produced basically the same results), and shows that the measured pressure profile fell between the adiabatic and isothermal predictions. Because of the double cushions, the branch pressures are approximately 30% less than that of the 30-in. line case, both analytically and experimentally.

Bottom/Side Arranged Tee

For the bottom/side arranged tee, the water fills the bottom branch first and then the side branch, thus generating a flow oscillation between branches. The branch flows and pressure losses are decided by the K-factor presented in Fig. 5. Figures 13 and 14 compare the analytical (adiabatic) and test results, respectively, for the bottom and the side branch of the 10- by 20- by 20-in. tee with initial ambient pressure. The pre-

dictions match the first bottom branch surge and the initial pressure rise of the side branch. The subsequent surges deviate somewhat from test data due to the adiabatic compression assumption and the tee's K-factor used in the analysis. Because the tee's K-factors are derived from steady-flow data and the gas may not behave adiabatically throughout, the predictions may deviate from test results.

Figures 15 and 16 compare the predictions to the test results, respectively, for the bottom and side branch of the same tee for the initial vacuum case. The prediction for the bottom branch was 23% higher than the test result and was only 2% higher for the side branch. The large deviation for the bottom branch may be the result of gas bubbles released from the water during the filling of the bottom branch. As the surge pressure wave propagates back to the bottom branch, the gas bubbles act like springs in the water, absorbing energy and reducing the surge pressure.

Test Repeatability

The tests were conducted at least three times for each test article and at each test condition. Test repeatability was very good for the straight line and elbow cases—a less than ±10% variation from the mean value. For example, the 30-in. line test case experienced only a ±2% variation for the initial vacuum case and a ±8% for the initial ambient case as shown in Fig. 17, which plots test data along with predictions (adiabatic and isothermal) for different initial line pressures. The percent variation increased as the flow oscillation between branches came into the picture; there was an approximately ±15% variation for the 10- by 10- by 10-in. right/left arranged tee case as shown in Fig. 18. The increase was mainly caused by the slightly uneven split flows at the tee junction. It should be emphasized here that identical or near identical peak branch pressures (i.e., even split flows) were recorded as shown in Fig. 18. For the 10- by 20- by 20-in. bottom/side arranged tee case, because of the rapid flow oscillation, the variation was ±25% for the initial vacuum case and ±10% for the initial ambient case. For a full-scale network system where branches are long, the large variation is not expected to occur.

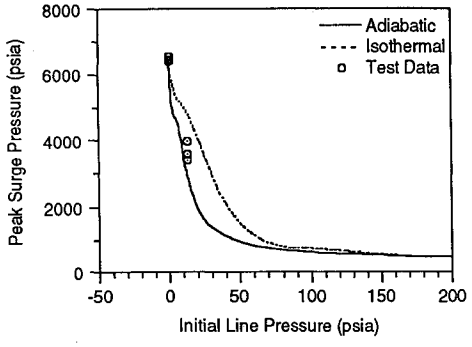

Fig. 17 30-in. line peak surge pressure comparison.

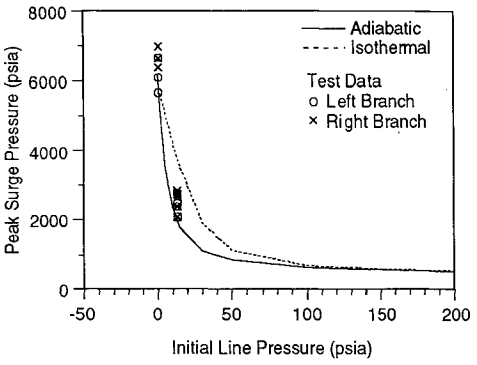

Fig. 18 10- × 10- × 10-in. right/left arranged tee peak surge pressure comparison.

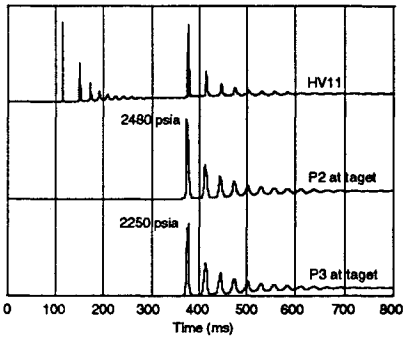

Fig. 19 Predictions for Prickett's Test Run no. 5.

Predictions for a Network Simulated Test Case

Prickett et al.[5] present network simulation tests that provide an opportunity to demonstrate the robustness of the analytical techniques presented here. Figure 19 shows the predictions for Test Run 5 (see Table 3, Prickett et al.[5]) which was chosen for its typical network configuration, consisting of a bottom/side arranged tee and a right/left arranged tee. The predictions show the pressure profiles at HV11, P2, and P3 (see Fig. 3, Prickett et al.[5] for locations) and indicate that the water impacted HV11 first at approximately 120 ms and then impacted P2 and P3 at approximately 370 ms. The measured impact times at P2 and P3 were 350 ms. The predicted peak pressures at P2 and P3 were 2480 and 2250 psia, respectively, which are 18 and 13% higher than the test results. The advantage of the analysis methods presented here is obvious; it allows the flow of a whole network to be simulated throughout the priming process, and predicts surge pressures throughout the system. Previous analysis methods[4,5] allowed only predictions of initial impact surge with no provision for the wave propagation and interaction that may easily double the initial impact surge as demonstrated in the 10- by 10- by 10-in. right/left arranged tee case. Only with the full consideration of momentum and continuity equations will the two main ingredients of the water-hammer effect, the inertia effect and the elastic effect, be accounted for in obtaining precise predictions of surge pressures.

Conclusions

A comprehensive technique for analyzing a propellant feed system priming process and a comparison of theory with experimental data was presented. The accuracy of the theoretical predictions has been well-assessed by the measured data both for the basic feed line configuration test articles and a network simulation test. The employed analytical modeling technique combined with the method of characteristics provides a full account of the water-hammer effect throughout the priming process of a propellant feed system.

Acknowledgment

The authors thank the White Sands Test Facility laboratory, Las Cruces, New Mexico, for the test data used in this article.

References

[1]Baker, D., Beeson, H., Benz, F., Fernandez, D., and Plaster, M., "Explosive Decomposition of Hydrazine by Rapid Compression of Gas Ullages," 1988 JANNAF Safety and Environmental Protection Subcommittee Meeting, Chemical Propulsion Information Agency, Johns Hopkins Univ., Laurel, MD, May 1988.

[2]Fritz, D. E., Dressler, G. A., and Mayer, N. L., "Development and Flight Qualification of the Propulsion and Reaction Control System for ERIS," AIAA Paper 92-3663, July 1992.

[3]Knowles, P. J., "Hydrazine Pressure Surges into an Evacuated Manifold Assembly," *Proceedings of the 1981 JANNAF Propulsion Meeting*, Vol. 1, CPIA Publication 340, Laurel, MD, 1981, pp. 607–627.

[4]Yaggy, K. L., "Analysis of Propellant Flow into Evacuated and Pressurized Lines," AIAA Paper 84-1346, June 1984.

[5]Prickett, R. P., Mayer, E., and Hermel, J., "Water Hammer in a Spacecraft Propellant Feed System," *Journal of Propulsion and Power*, Vol. 8, No. 3, 1992, pp. 592–597.

[6]Wylie, E. B., and Streeter, V. L., *Fluid Transients* (corrected edition), FEB Press, Ann Arbor, MI, 1983, pp. 17–23.

[7]Vazsonyi, A., "Pressure Loss in Elbows and Duct Branches," *Transactions of the American Society of Mechanical Engineers*, Vol. 66, April 1944, pp. 177–183.

[8]"Screwed End Port Entry Ball Valves," Bulletin B180, Neles-Jamesbury Co., Worcester, MA, Nov. 1971.